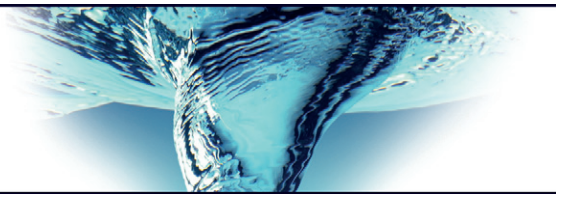
*J. Fluid Mech.* (2019), *vol.* 878, R5, doi:10.1017/jfm.2019.730



JFM RAPIDS
journals.cambridge.org/rapids

# A stable tripole vortex model in two-dimensional Euler flows

**A. Viúdez**†

Department of Physical Oceanography and Technology, Institute of Marine Sciences, CSIC, Barcelona 08003, Spain

(Received 3 June 2019; revised 9 July 2019; accepted 30 August 2019;
first published online 17 September 2019)

An exact solution of a stable vortex tripole in two-dimensional (2-D) Euler flows is provided. The stable tripole is composed of an inner elliptical vortex and two small-amplitude lateral vortices. The non-vanishing vorticity field of this tripole, referred to as here as an embedded tripole because of the closeness of its vortices, is given in elliptical coordinates $(\mu, \nu)$ by the even radial and angular order-0 Mathieu functions $\mathrm{Je}_0(\mu)\mathrm{ce}_0(\nu)$ truncated at the external branch of the vorticity isoline passing through the two critical points closest to the vortex centre. This tripole mode has a rigid vorticity field which rotates with constant angular velocity equal to $\zeta_0\mathrm{Je}_0(\mu_1)\mathrm{ce}_0(0)/2$, where $\mu_1$ is the first zero of $\mathrm{Je}_0'(\mu)$ and $\zeta_0$ is a constant modal amplitude. It is argued that embedded 2-D tripoles may be conceptually regarded as the superposition of two asymmetric Chaplygin–Lamb dipoles, separated a distance equal to $2R$, as long as their individual trajectory curvature radius $R$ is much shorter than their dipole extent radius.

**Key words:** vortex dynamics, vortex instability, vortex interactions

## 1. Introduction

Stable two-dimensional (2-D) tripolar vortex structures usually emerge from unstable axisymmetric vortices in homogeneous fluids (van Heijst & Kloosterziel 1989; van Heijst, Kloosterziel & Williams 1991). These tripoles are the equilibrium state reached, through an unsteady flow process, from initial unstable conditions (Carton, Flierl & Polvani 1989; Orlandi & van Heijst 1992). The persistence of this final equilibrium state supports the high stability of these tripolar structures and encourages the search for mathematical models that could explain their physical properties (Kizner & Khvoles 2004). The name vortex tripole, though it always refers to three vortices of alternate vorticity located along a common straight line, is applied to at least two different 2-D vortex structures. A first acceptation refers to tripoles as composed by one central vortex surrounded by satellite vortices of opposite vorticity orbiting

† Email address for correspondence: aviudez@cmima.csic.es

© Cambridge University Press 2019



https://doi.org/10.1017/jfm.2019.730 Published online by Cambridge University Press

around the central vortex (as in Polvani & Carton (1990), henceforth referred to as orbital tripoles). In this case there is a relatively large distance between vortices and, as a consequence, a small vorticity gradient among them. A second acceptation refers to those tripoles embedded in the same vortex structure (as in Kizner & Khvoles (2004), henceforth referred to as embedded tripoles). In this case the side vortices are of small amplitude, and their shape is highly curved due to their closeness to the central vortex. The objective of work is to provide exact piecewise mathematical solutions of steadily rotating and stable embedded tripoles with rigid distributed vorticity in 2-D Euler flows.

The basic equations are briefly introduced in § 2. In circular geometry, the steady solutions, or steadily rotating with rigid vorticity solutions, to the material conservation of vorticity lead to the Helmholtz equation in polar coordinates, whose solutions are the Bessel azimuthal normal modes. Among all the modes only the order 0 and order 1 are stable modes. The superposition of these modes is the steadily rotating with rigid distributed vorticity 2-D Chaplygin–Lamb (C–L) dipole (Lamb 1895; Chaplygin 1903; Flierl, Stern & Whitehead 1983; Meleshko & van Heijst 1994). The interior C–L vorticity solution consists in the sum of the first two Bessel normal modes: namely, the mode-0, or circular mode, $\phi_0 \mathrm{J}_0(r)$, and the mode-1, or dipolar mode, $\phi_1 \mathrm{J}_1(r)\cos\theta$, with constant modal amplitudes $\{\phi_0, \phi_1\}$. Though the stability of the C–L dipole suggests that more Bessel modes, $\phi_n \mathrm{J}_n(r)\cos(n\theta)$, could be added to find steadily rotating tripole solutions, the mode-$n$ involves $n$ vortex dipoles which are dispersive modes for $n \geqslant 2$ (Viúdez 2019). Thus, no combination of Bessel normal modes represents a steady and stable solution and, consequently, exact solutions of 2-D stable embedded tripoles are not azimuthal-mode streamfunction solutions $\phi(r, \theta)$ of the Helmholtz equation $\nabla^2\phi = -k^2\phi$ in polar coordinates $(r, \theta)$ assuming a circular vortex geometry, and solutions with a different vortex geometry should be investigated.

However, the C–L dipole, due to its high stability, could be considered the building block of more complex steady 2-D vortex structures, and it is reasonable to think that it should play a relevant role, at least conceptually, in steady embedded tripole models. Such a conceptual C–L dipole model of an embedded tripole is possible and is described in § 3. The C–L dipole has a non-dimensional radius given by the first zero $j_{1,1} \simeq 3.83$ of the Bessel function of order one, $\mathrm{J}_1(r)$. Given the fundamental property that an isolated C–L dipole describes a circular trajectory with a curvature radius $R_0 = |\phi_1/\phi_0|$, dipoles with a small dipolar amplitude ratio such that $|\phi_1/\phi_0| < j_{1,1}$ have a rotation centre located inside the vortex. It is therefore possible to build a tripole model by superposing two C–L dipoles with small amplitude ratio and an angular phase shift $\Delta\theta = \pi$, and whose dipole centres are initially separated a distance $2R_0$. Since the C–L dipoles have rigid vorticity fields, this two-dipole tripole model is expected to rotate, with small deformation from its initial vorticity state, around the origin point. Due to the nonlinear interaction between the two C–L dipoles, this tripole model is not steady, but it quickly evolves towards a rigid vorticity field, rotating with constant angular vorticity and whose inner vorticity isolines are ellipses. This geometrical result leads us then to construct a steady tripole model (§ 4) based on the eigenfunctions of the Laplacian operator in elliptic coordinates – namely, the Mathieu functions. The resulting tripole with continuous distributed vorticity is a piecewise vorticity solution whose inner, non-vanishing, vorticity field is given by the Mathieu functions of order zero and even symmetry. The tripole extent is limited by the external branch of the vorticity isoline, or tripole separatrix, passing through the two critical, stagnation points closest to the vortex centre. The value of this vorticity



https://doi.org/10.1017/jfm.2019.730 Published online by Cambridge University Press

isoline determines the angular velocity of the tripole. Numerical simulations confirm that this embedded tripole model rotates with rigid vorticity with the predicted frequency, as well as suggesting its long-term stability. Finally, concluding remarks are given in § 5.

## 2. Basic dynamical equations

In 2-D isochoric Euler flows the field solutions are given in terms of a stream-function $\psi(\boldsymbol{x}, t)$ which provides the horizontal velocity $\boldsymbol{u}(\boldsymbol{x}, t)$ and vorticity $\zeta(\boldsymbol{x}, t)$ fields,

$$\boldsymbol{u} = -\boldsymbol{\nabla} \times (\psi \boldsymbol{k}), \quad \zeta \equiv \boldsymbol{k} \cdot \boldsymbol{\nabla} \times \boldsymbol{u} = \nabla^2 \psi, \tag{2.1a,b}$$

where $\boldsymbol{k}$ is the vertical unit vector and $\boldsymbol{\nabla}$ is the 2-D gradient operator. The fundamental dynamical equation is the material conservation of vorticity

$$\frac{\mathrm{d}\zeta}{\mathrm{d}t} = \frac{\partial \zeta}{\partial t} + \boldsymbol{u} \cdot \boldsymbol{\nabla} \zeta = \frac{\partial}{\partial t} \nabla^2 \psi + \mathcal{J}\{\psi, \nabla^2 \psi\} = 0, \tag{2.2}$$

where $\mathcal{J}\{A(x, y), B(x, y)\} \equiv \partial A/\partial x \partial B/\partial y - \partial B/\partial x \partial A/\partial y$ is the Jacobian operator.

## 3. The two-dipole vortex as a conceptual embedded tripole model

Though it is possible to form an initial tripolar vortex structure, in polar coordinates $(r, \theta)$, with boundary radius $r = j_{1,1}$, from a combination of circular Bessel modes 0 and 2 in the form $\zeta(r, \theta) = \zeta_0[\mathrm{J}_0(r) - \mathrm{J}_0(j_{1,1})] + \zeta_2 \mathrm{J}_2(k_0 r) \cos(2\theta)$, this vorticity structure is unstable (see figure 3 and explanation in Viúdez (2019)). In the above, $\mathrm{J}_i(r)$ is the Bessel function of the first kind and order $i$, $j_{i,m}$ is the $m$-zero of $\mathrm{J}_i(r)$, $\{\zeta_0, \zeta_2\}$ are the real constant modal amplitudes, and the constant $k_0 \equiv j_{2,1}/j_{1,1}$ so that at the vortex boundary $\mathrm{J}_2(k_2 j_{1,1}) = \mathrm{J}_2(j_{2,1}) = 0$. This instability occurs because, in a vortex, azimuthal mode-2 (as it happens to any azimuthal mode $i \geqslant 2$, which may be thought of as consisting of $i$ dipoles) is a dispersive mode in the sense that the two dipoles, located inside a circle, tend to move apart, breaking the vortex, and disperse when mode-2 dominates ($|\zeta_2| \gg |\zeta_0|$). When mode-0 dominates ($|\zeta_0| \gg |\zeta_2|$), the mode-1 perturbation is circularly advected by the circular mode-0 and spiralizes so that its radial wavenumber increases indefinitely. In numerical simulations this perturbation is eventually dumped by numerical diffusion. When both amplitudes $|\zeta_0|$ and $|\zeta_2|$ are of the same order of magnitude, the unsteady vortex may evolve up to an orbital tripole vortex; although this occurs through a severe unsteady rearrangement of the vorticity field.

However, there is a way to assemble an embedded tripole from the superposition of two C–L dipoles. It is well known that an asymmetric circular C–L dipole (subscript $D$) whose initial non-vanishing piecewise vorticity distribution is given by

$$\hat{\zeta}_D(r, \theta; \theta_0) \equiv \zeta_0[\mathrm{J}_0(r) - \mathrm{J}_0(j_{1,1})] + \zeta_1 \mathrm{J}_1(r) \cos(\theta + \theta_0), \quad r \leqslant j_{1,1}, \tag{3.1}$$

rotates rigidly with constant angular velocity $\Omega_0 = -\zeta_0 \mathrm{J}_0(j_{1,1})/2$, describing a circular trajectory with radius $R_0 = |\zeta_1/\zeta_0|$. Consider now a small dipolar amplitude $|\zeta_1| < j_{1,1}|\zeta_0|$ so that the trajectory curvature radius $R_0$ is shorter than the dipole extent radius $j_{1,1}$. In this case the dipole's motion would resemble that of a vortex with one vorticity anomaly patch spinning with angular velocity $\Omega_0$ around the inner core vortex. We superpose to this vorticity field the vorticity field of a twin dipole but with a phase shift $\Delta\theta_0 = \pi$ and whose vortex centre is separated a distance



https://doi.org/10.1017/jfm.2019.730 Published online by Cambridge University Press

$2R_0$ from its twin vortex dipole centre. Considered in isolation, these C–L dipoles rotate with the same angular velocity around the origin point. It is convenient now to work simultaneously with both polar $(r, \theta)$ and Cartesian $(x, y)$ coordinates because the dipole internal structure is naturally defined in polar coordinates, while the dipole's location is expressed more easily in Cartesian coordinates. Let the vorticity distribution in Cartesian $(x, y)$ coordinates of the C–L vortex dipole be

$$\tilde{\zeta}_D(x, y; \theta_0) = \hat{\zeta}_D(r(x, y), \theta(x, y); \theta_0), \tag{3.2}$$

where the usual Cartesian to polar coordinates transformations are $r(x, y) = \sqrt{x^2 + y^2}$ and $\theta(x, y) = \arctan y/x$. For ease of reference denote the non-vanishing vorticity fields, in Cartesian coordinates, of the right (subscript $R$) and left (subscript $L$) twin dipoles as

$$\tilde{\zeta}_{DR}(x, y) \equiv \tilde{\zeta}_D(x + R_0, y; 0), \quad r(x + R_0, y) \leqslant j_{1,1}, \tag{3.3}$$

$$\tilde{\zeta}_{DL}(x, y) \equiv \tilde{\zeta}_D(x - R_0, y; \pi), \quad r(x - R_0, y) \leqslant j_{1,1}. \tag{3.4}$$

Thus, the non-vanishing initial piecewise vorticity field of the two-dipole tripole model (subscript $T$) is

$$\tilde{\zeta}_T(x, y) \equiv \tilde{\zeta}_{DR}(x, y) + \tilde{\zeta}_{DL}(x, y). \tag{3.5}$$

Since, in isolation, the twin dipoles rotate with the same angular velocity $\Omega_0 = -\zeta_0 \mathrm{J}_0(j_{1,1})/2$ describing a circle of radius $R_0$ it is expected that at a first, linear approximation, the vortex tripole structure (3.5) would rotate steadily with twice the angular velocity $\Omega_T = -(2\zeta_0)\mathrm{J}_0(j_{1,1})/2$, because the two C–L amplitudes are added, around the geometrical centre of the two dipoles (the origin point $(x, y) = (0, 0)$).

We calculate next the different terms in the vorticity conservation balance (2.2). To do so it is convenient, in order to avoid the irrelevant advection of the rigid vorticity field, to work in the reference frame rotating with angular velocity $\Omega_0$ in which the C–L dipoles are steady. In this co-rotating reference frame the dipole vorticity $\widehat{\zeta}_D$ is $\hat{\zeta}_D$ given by (3.1) minus the vorticity of the rotating frame $(2\Omega_0 = -\zeta_0 \mathrm{J}_0(j_{1,1}))$, that is

$$\widehat{\zeta}_D(r, \theta; \theta_0) \equiv \begin{cases} \zeta_0 \mathrm{J}_0(r) + \zeta_1 \mathrm{J}_1(r) \cos(\theta + \theta_0), & r \leqslant j_{1,1} \\ \zeta_0 \mathrm{J}_0(j_{1,1}), & j_{1,1} \leqslant r. \end{cases} \tag{3.6}$$

We further define, in analogy to the previous definitions, in the co-rotating reference frame and in Cartesian coordinates the circular dipole

$$\widetilde{\zeta}_D(x, y; \theta_0) = \widehat{\zeta}_D(r(x, y), \theta(x, y); \theta_0), \tag{3.7}$$

and the right $\widetilde{\zeta}_{DR}(x, y)$ and left $\widetilde{\zeta}_{DL}(x, y)$ dipoles are defined as (3.3) and (3.4), respectively. Finally, the two-dipole tripole vorticity model is given by

$$\widetilde{\zeta}_T(x, y) \equiv \widetilde{\zeta}_{DR}(x, y) + \widetilde{\zeta}_{DL}(x, y), \tag{3.8}$$

and is displayed in figure 1(*a*). The superposition of the two piecewise vorticity C–L dipole distributions defines four regions in the tripole domain: one inner region, defined as the intersection of the two interior vorticity dipole domains; two lateral regions ($L$ and $R$), occupied by only one interior dipole ($L$ or $R$) domain; and one outer region, defined as the intersection of the two exterior vorticity dipole domains.



https://doi.org/10.1017/jfm.2019.730 Published online by Cambridge University Press

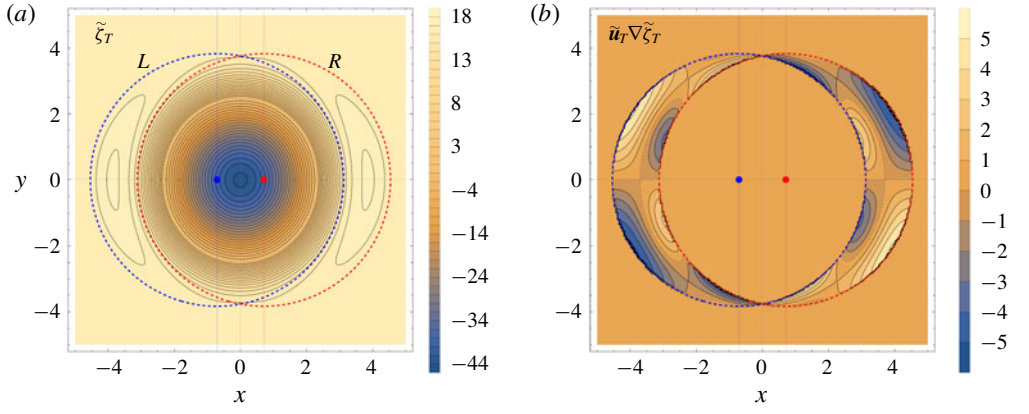



FIGURE 1. (*a*) The piecewise vorticity $\widetilde{\zeta}_T(x, y)$ $(\times 20)$ of the two-dipole tripole model with modal amplitudes $\zeta_0 = -1$ and $\zeta_1 = -1/\sqrt{2}$. The blue and red solid circles define, respectively, the boundaries of the left ($L$) and right ($R$) C–L dipoles. Contour intervals $\Delta_\zeta = 1$ for $\widetilde{\zeta}_T < 0$ and $\Delta_\zeta = 2$ for $\widetilde{\zeta}_T > 0$. (*b*) Advection of the two-dipole tripole model $\widetilde{\boldsymbol{u}}_T \cdot \boldsymbol{\nabla}\widetilde{\zeta}_T$ $(\times 2 \times 10^3)$. Contour interval $\Delta = 1$.

In order to find up to what extent the two-dipole tripole (3.8) is a steadily rotating solution to the nonlinear equation of material conservation of vorticity (2.2) we calculate next the different advection terms involved. Since the product of the Bessel functions with the azimuthal modes, $\psi_n(r, \theta) \equiv \mathrm{J}_n(r)\exp(\mathrm{i}n\theta)$, are the eigenfunctions of the Laplacian in polar coordinates, $\nabla^2\psi_n = -\psi_n$, the advection of vorticity of every mode, given by the Jacobian $\mathcal{J}\{\psi_n, \nabla^2\psi_n\}$ in (2.2), vanishes. The nonlinear advection involving two modes $i$, $j$ also cancels out since $\mathcal{J}\{\psi_i, \nabla^2\psi_j\} = -\mathcal{J}\{\psi_j, \nabla^2\psi_i\}$. Thus, the advection of vorticity in the isolated dipole vanishes and the C–L dipole remains steady. The advection of vorticity vanishes as well in the interior tripole when the two dipoles are simultaneously present, because the advection involving any pair of modes $i, j \in \{0, 1\}$ includes the vortex crossing terms

$$\widetilde{\boldsymbol{u}}_{Li} \cdot \boldsymbol{\nabla}\widetilde{\zeta}_{Rj} + \widetilde{\boldsymbol{u}}_{Rj} \cdot \boldsymbol{\nabla}\widetilde{\zeta}_{Li} = \mathcal{J}\{\widetilde{\phi}_{Li}, -\widetilde{\phi}_{Rj}\} + \mathcal{J}\{\widetilde{\phi}_{Rj}, -\widetilde{\phi}_{Li}\} = 0. \tag{3.9}$$

We note that other vortex models, such as the Lamb–Oseen or Batchelor vortices, do not satisfy this superposition property. The vorticity advection in the exterior tripole vanishes as well, since the exterior vorticity is constant. Therefore, there remains only the vorticity advection in the lateral regions, or lateral vortices, which in the left lateral vortex is due to the advection of the $L$ vortex vorticity by the $R$ vortex velocity $\widetilde{\boldsymbol{u}}_R \cdot \boldsymbol{\nabla}\widetilde{\zeta}_L$, and in the right lateral vortex is due to the advection of the $R$ vortex vorticity by the $L$ vortex velocity $\widetilde{\boldsymbol{u}}_L \cdot \boldsymbol{\nabla}\widetilde{\zeta}_R$. For example, we may check (appendix A) that the vorticity advection in the left lateral region is

$$\widetilde{\boldsymbol{u}}_R \cdot \boldsymbol{\nabla}\widetilde{\zeta}_L(x, y) = \frac{y\phi_1^2 \mathrm{J}_0(j_{1,1})}{2(x_-^2 + y^2)^2}\left[(x_+)\frac{(x_-^2 + y^2)^2 - j_{1,1}^2(x_-^2 + y^2 - 4R_0x_-)}{x_+^2 + y^2}\mathrm{J}_2\left(\sqrt{x_+^2 + y^2}\right)\right.$$
$$\left. + (x_-)\frac{2j_{1,1}^2}{\sqrt{x_+^2 + y^2}}\mathrm{J}_1\left(\sqrt{x_+^2 + y^2}\right)\right], \tag{3.10}$$



https://doi.org/10.1017/jfm.2019.730 Published online by Cambridge University Press

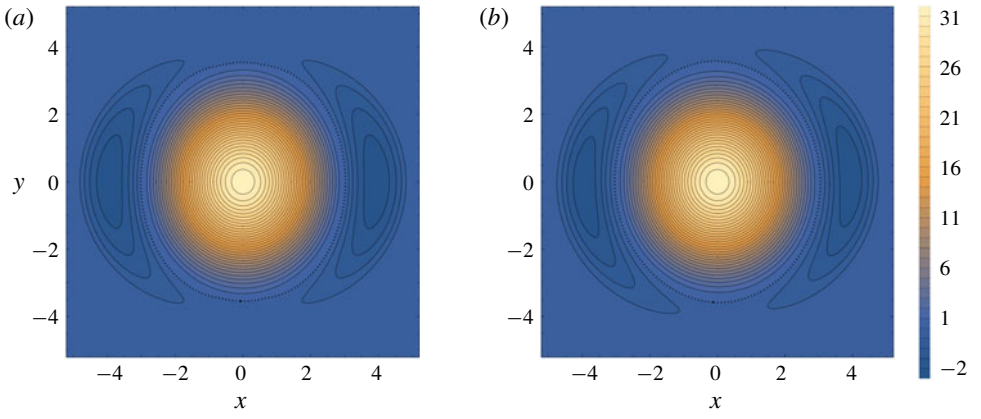



FIGURE 2. The vorticity distribution $\tilde{\zeta}_T(x, y, t_0)$ ($\times 20$) from numerical simulations of the two-dipole tripole model, with amplitudes $\zeta_0 = \zeta_1 = 1/2$, at (*a*) $t_0 = 0$, and (*b*) $t_0 = 500$. Contour intervals $\Delta_\zeta = 0.5$ ($\tilde{\zeta}_T < 0$) and $\Delta_\zeta = 1$ ($\tilde{\zeta}_T > 0$). The black thick dotted line is the contour $\tilde{\zeta}_T = 0$. The background numerical vorticity is $\bar{\zeta}_N \simeq -0.02064$.

where $x_\pm \equiv x \pm \phi_1/\phi_0$. The complete vorticity advection distribution is shown in figure 1(*b*). The vorticity advection (3.10) vanishes for $\phi_1 = 0$ (this case lacks the dipolar mode, $R_0 = 0$), vanishes also along the axis $y = 0$, and depends linearly on $\phi_1^2$, which is assumed small compared to $\phi_0^2$. Note that (3.10) depends on $\phi_0$ through $x \pm \phi_1/\phi_0$ and $R_0 \equiv \phi_1/\phi_0$. We recall that when the two vorticity fields are added in (3.8) the constant background vorticity field is doubled to $2\zeta_0 \mathrm{J}_0(j_{1,1})$, and therefore the two-dipole tripole model is expected to rotate with an angular velocity $\Omega_T = -\zeta_0 \mathrm{J}_0(j_{1,1})$.

Numerical simulations were carried out using a 2-D pseudo-spectral code where the vorticity field $\zeta(x, y, t)$ is numerically integrated in a double-periodic domain using an explicit leap-frog time-stepping method, together with a weak Robert–Asselin time filter to avoid the decoupling of even and odd time levels (as in Dritschel & Viúdez 2003). Spatial fields are computed using the pseudo-spectral method, wherein spatial derivatives are computed in spectral space, while the advective nonlinear products are computed on the physical grid, and fast Fourier transforms are used to go from one representation to the other. Numerical simulations with a moderate resolution ($1024^2$ grid points), initialized with the two-dipole tripole vorticity distribution (figure 2*a*) confirmed that the tripole was stable and soon reaches a rigidly rotating vorticity field (figure 2*b* and supplementary movie 1, available at https://doi.org/10.1017/jfm.2019.730). In a time period $\Delta_T = 500$ the tripole undergoes $N_R = 29/2$ anticlockwise rotations. Since the numerical pseudo-spectral algorithm requires zero spatial average vorticity there is a small background constant vorticity in figure 2 equal to $\bar{\zeta}_N \simeq -0.02064$, which provides a small correction to the tripole angular velocity $\Omega_T = 2\pi N_R/\Delta_T - \bar{\zeta}_N/2 \simeq 0.1822 + 0.0103 \simeq 0.192$. This angular velocity compares well with the angular velocity of an isolated C–L dipole, with double mode-0 amplitude, $\Omega_T = -\zeta_0 \mathrm{J}_0(j_{1,1}) \simeq 0.201$.

It is also possible to construct asymmetric tripoles selecting different modal amplitudes $\phi_{L0} \neq \phi_{R0}$ for the left ($L$) and $\phi_{L1} \neq \phi_{R1}$ for the right ($R$) C–L dipoles. For example, setting without loss of generality $\phi_{L0} = 1$, and positive modal amplitudes such that the left $R_L \equiv \phi_{L0}/\phi_{L1}$ and right $R_R \equiv \phi_{R0}/\phi_{R1}$ C–L dipole trajectory radius



https://doi.org/10.1017/jfm.2019.730 Published online by Cambridge University Press

coincide ($R_L = R_R$), with $\phi_{L1} \neq \phi_{R1}$, leads to steadily rotating asymmetric tripoles whose centre (the point where vorticity reaches an extremum) remains approximately at the origin point. Positive modal amplitudes such that the left and right C–L dipole trajectory radius differ ($R_L \neq R_R$) lead to asymmetric tripoles whose centre approximately describes circles around the origin point. Asymmetric fixed-centre tripoles ($R_L = R_R$) were found to be numerically more stable than the asymmetric rotating-centre tripoles ($R_L \neq R_R$).

Considering the simplicity of the symmetric two-dipole tripole distribution, it is surprising that the numerical simulations show very similar initial and steadily rotating vorticity distributions (figure 2). This implies that the two-dipole tripole model is a reasonably good conceptual model of an embedded tripole. A closer look at largely augmented images of the time-evolving interior vorticity isolines reveals that their shapes change until reaching, in the steadily rotating state (figure 2*b*), a confocal elliptical geometry. This fact suggests the search for steady and stable elliptical vortex tripoles carried out in the next section.

## 4. Steadily rotating tripole model with distributed vorticity

This section provides exact solutions, with continuous vorticity, of stable and steadily rotating embedded tripole vortices. Guided by the results obtained in the previous section using the two-dipole tripole model we look for steady streamfunction solutions $\phi(\mu, \nu) = R(\mu)\Phi(\nu)$ separable in elliptic coordinates $(\mu, \nu)$ with $0 \leqslant \mu < \infty$ and $-\pi \leqslant \nu < \pi$. Elliptic coordinates $(\mu, \nu)$ are defined through the usual relation to Cartesian coordinates $(x, y)$:

$$x(\mu, \nu; f) = f \cosh\mu \cos\nu, \quad y(\mu, \nu; f) = f \sinh\mu \sin\nu, \tag{4.1a,b}$$

where the two foci are located at $(x, y) = (\pm f, 0)$. Thus, the streamfunction $\phi(\mu, \nu)$ must satisfy (2.2) in the steady state, which becomes the Helmholtz equation in elliptic coordinates,

$$\nabla^2\phi(\mu, \nu) = \frac{\phi_{\mu\mu}(\mu, \nu) + \phi_{\nu\nu}(\mu, \nu)}{f^2(\sinh^2\mu + \sin^2\nu)} = -k^2\phi(\mu, \nu), \tag{4.2}$$

where $k$ is the wavenumber. The solutions of (4.2) are the ordinary (angular) and the modified (radial) Mathieu equations (see, for example, McLachlan 1951; Abramowitz & Stegun 1964; Gutiérrez-Vega *et al.* 2003)

$$\Phi''(\nu) + (a - 2q\cos 2\nu)\Phi(\nu) = 0, \tag{4.3}$$

$$R''(\mu) - (a - 2q\cosh 2\mu)R(\mu) = 0, \tag{4.4}$$

where $a$ is the separation constant and $q \equiv f^2k^2/4$. The angular Mathieu equation (4.3) has two families of independent solutions: namely the even, cosine-elliptic angular Mathieu functions $\Phi_m(\nu) = \mathrm{ce}_m(\nu; q)$, $m = 0, 1, 2, \ldots$, and the odd, sine-elliptic angular Mathieu functions $\Phi_m(\nu) = \mathrm{se}_m(\nu; q)$, $m = 1, 2, \ldots$, where $m$ is the order. The value of the separation constant $a = a_r(r; q)$ that satisfies the angular periodicity conditions is the characteristic value for the even Mathieu function with characteristic exponent $r$ and parameter $q$. When $q > 0$ the solutions $R_m(\mu)$ to (4.4) are the even (e) and odd (o) oscillatory radial Mathieu functions of the first kind (Je$(\mu; q)$ and Jo$(\mu; q)$) and second kind (Ne$(\mu; q)$ and No$(\mu; q)$).



https://doi.org/10.1017/jfm.2019.730 Published online by Cambridge University Press

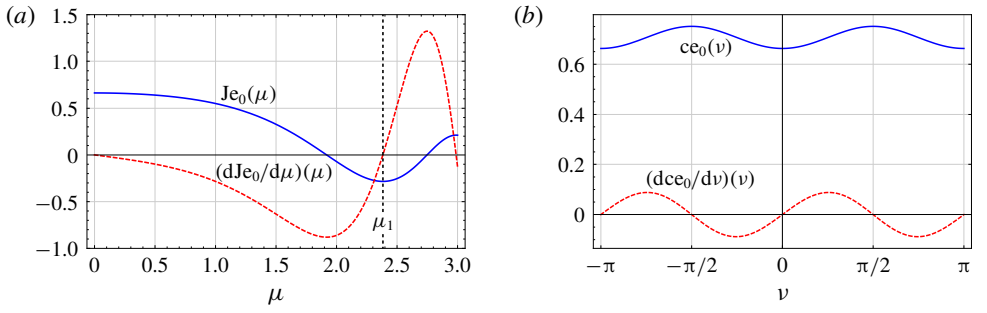



FIGURE 3. The even order-0 Mathieu functions and their derivatives. (*a*) Radial functions $\mathrm{Je}_0(\mu)$ and $\mathrm{Je}_0'(\mu)$. The first zero $\mu_1 \simeq 2.3833$ of $\mathrm{Je}_0'(\mu)$ is indicated. (*b*) Angular functions $\mathrm{ce}_0(\nu)$ and $\mathrm{ce}_0'(\nu)$. Function $\mathrm{ce}_0(\nu)$ is similar to a shifted $-\cos 2\nu$ function. Parameter $q = 1/8$ corresponding to $f = 1/\sqrt{2}$ and $k = 1$.

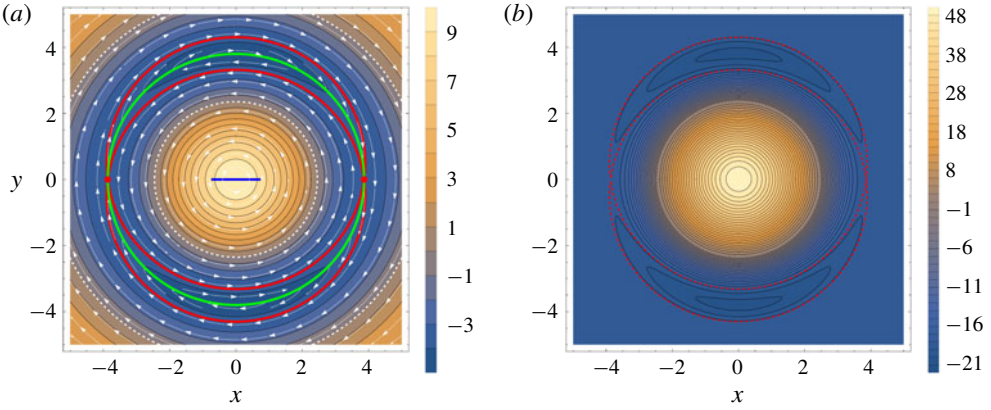



FIGURE 4. (*a*) Mathieu distribution $\mathrm{Je}_0(\mu(x,y);q)\mathrm{ce}_0(\nu(x,y);q)$ ($\times 20$, thin black contours) for wavenumber $k = 1$ and foci $f = 1/\sqrt{2}$. The blue horizontal line joins the foci points $(\pm f, 0)$. The white lines with arrows are the streamlines of (4.6). The two red dots are the critical points $(\mu, \nu) = (\mu_1, 0)$ and $(\mu, \nu) = (\mu_1, \pi)$. The green curve is the ellipse $\mu(\nu) = \mu_1$ passing through the critical points. The red curves are the isolines of $\mathrm{Je}_0(\mu)\mathrm{ce}_0(\nu) = \mathrm{Je}_0(\mu_1)\mathrm{ce}_0(0)$. (*b*) The piecewise vorticity field $\zeta(x,y) = \mathrm{Je}_0(\mu)\mathrm{ce}_0(\nu)$ $(\mu \leqslant \mu_B(\nu))\zeta(x,y) = \mathrm{Je}_0(\mu_1)\mathrm{ce}_0(0)$ $(\mu > \mu_B(\nu))$, ($\times 20$, thin black contours). Contour intervals are $\Delta_\zeta = 1$ $(\zeta < 0)$ and $\Delta_\zeta = 2$ $(\zeta > 0)$. The white thin dotted contour is the zero-vorticity isoline. The red dashed curves are the isolines of $\zeta = \mathrm{Je}_0(\mu_1)\mathrm{ce}_0(0)$.

The interior vorticity $\zeta_i(\mu, \nu)$ of the tripole vortex model introduced here is given by the simplest mode, namely the even order-0 Mathieu functions of the first kind

$$\zeta_i(\mu, \nu; q) = -\phi_i(\mu, \nu; q) = \zeta_0 \mathrm{Je}_0(\mu; q)\mathrm{ce}_0(\nu; q). \tag{4.5}$$

The order-0 radial and angular Mathieu functions $\mathrm{Je}_0(\mu)$ and $\mathrm{ce}_0(\nu)$ are shown in figure 3, and the corresponding field solution $\mathrm{Je}_0(\mu; q)\mathrm{ce}_0(\nu; q)$ in figure 4(*a*). The interior velocity is

$$\boldsymbol{u}_i(\mu, \nu) = -\boldsymbol{\nabla} \times (\phi_i(\mu, \nu)\boldsymbol{k}) = \frac{-\mathrm{Je}_0(\mu)\mathrm{ce}_0'(\nu)\boldsymbol{e}_\mu + \mathrm{Je}_0'(\mu)\mathrm{ce}_0(\nu)\boldsymbol{e}_\nu}{f\sqrt{\sinh^2\mu + \sin^2\nu}}. \tag{4.6}$$



https://doi.org/10.1017/jfm.2019.730 Published online by Cambridge University Press

The boundary separating the interior vortical flow from the exterior potential flow, say curve $\mu = \mu_B(\nu)$, is set as the external branch (external red curve in figure 4*a*) of the vorticity isoline passing through the first critical points $(\mu_1, 0)$ and $(\mu_1, \pi)$, where $\mu_1$ is the first minimum of $\mathrm{Je}_0(\mu)$, or first zero (excluding $\mu = 0$) of $\mathrm{Je}_0'(\mu)$ (figure 3*a*). Thus, the separatrix vorticity value is

$$\zeta(\mu_B(\nu), \nu) = \zeta(\mu_1, 0) = \zeta_l \simeq 0.1879. \tag{4.7}$$

The other relevant curve passing through the critical points is a vorticity extremum and is the ellipse $\mu(\nu) = \mu_1$ (green curve in figure 4*a*). Along this curve $\mathrm{Je}_0'(\mu_1) = 0$ and the velocity has only a $\mu$-component,

$$\boldsymbol{u}(\mu_1, \nu) = -\frac{\mathrm{Je}_0(\mu_1)\mathrm{ce}_0'(\nu)}{f\sqrt{\sinh^2\mu_1 + \sin^2\nu}}\,\boldsymbol{e}_\mu. \tag{4.8}$$

Finally, the non-vanishing vorticity of the embedded tripole is given, in the fixed reference frame at the initial time $t_0 = 0$, by

$$\zeta(\mu, \nu, t_0) = \zeta_0(\mathrm{Je}_0(\mu)\mathrm{ce}_0(\nu) - \mathrm{Je}_0(\mu_1)\mathrm{ce}_0(0)), \quad \mu \leqslant \mu_B(\nu). \tag{4.9}$$

In the case of approaching circular geometry ($f \to 0$) the radial Mathieu functions $\mathrm{Je}_n(\mu)$ converge to the Bessel functions $\mathrm{J}_n(r)$, curves $\mu = \mu_B(\nu)$ and $\mu = \mu_1$ collapse to the circle of radius $r = j_{1,1} \simeq 3.8317$, and the tripole converges to the circular mode of the C–L dipole. Since $\mathrm{J}_0'(r) = -\mathrm{J}_1(r)$, the C–L dipole has, at its boundary radius $r = j_{1,1}$, both vanishing radial velocity, given by $\mathrm{J}_0'(j_{1,1}) = -\mathrm{J}_1(j_{1,1}) = 0$, and constant vorticity, given by $\mathrm{J}_0(j_{1,1})$. This is not, however, the case in the embedded vortex tripole.

The complicated boundary conditions at $\mu = \mu_B(\nu)$ make it difficult to find a closed-form solution of the exterior streamfunction, which is not provided here. The exterior streamfunction, however, can always be obtained numerically from the inversion of $\zeta = -\nabla^2\phi$, which is straightforward using the 2-D Fourier transform in a rectangular domain. Numerical simulations using a pseudo-spectral code with $2048^2$ grid points confirmed the stability of the embedded tripole (supplementary movie 2) after some time adjustment in the lateral vortices related to the instability at the critical points. In a time interval $\Delta_T = 4240$ (figure 5) the tripole performed $N_R = 60$ rotations, which, taking into account a small background constant numerical vorticity $\bar{\zeta}_N \simeq -0.00331$, results in an angular velocity $\Omega_0 = 2\pi N_R/\Delta_T - \bar{\zeta}_N/2 \simeq 0.0889 + 0.00166 \simeq 0.091$. This value compares well with the theoretical angular velocity $\zeta_l/2 = \mathrm{Je}_0(\mu_1)\mathrm{ce}_0(0)/2 \simeq 0.094$.

## 5. Concluding remarks

We have found exact solutions of steady and stable 2-D tripoles with distributed vorticity and small-amplitude embedded lateral vortices. The solutions are given in elliptical coordinates $(\mu, \nu)$ by the even radial and angular Mathieu function of order zero $\mathrm{Je}_0(\mu)\mathrm{ce}_0(\nu)$ truncated at the external branch of the first separation streamline. The tripole rotates with an angular velocity $\Omega_0 = -\zeta_0\mathrm{Je}_0(\mu_1)\mathrm{ce}_0(0)/2 \simeq 0.09397\zeta_0$, where $\mu_1$ is the first zero of $\mathrm{Je}_0'(\mu)$. Although, due to the difficulties associated with the Mathieu functions, this tripole model is difficult to handle, it is possible to conceptually think of embedded 2-D tripoles as the superposition of two C–L dipoles separated a distance equal to twice the distance of their individual trajectory curvature



https://doi.org/10.1017/jfm.2019.730 Published online by Cambridge University Press

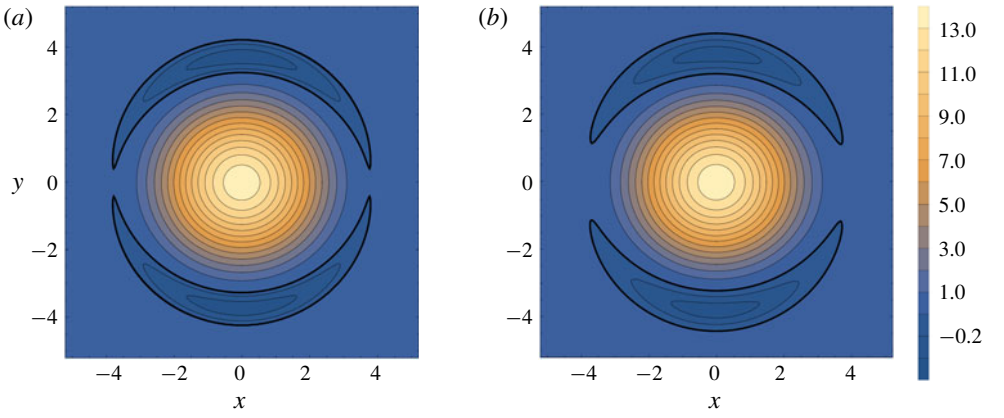



FIGURE 5. The piecewise vorticity $\zeta(x, y, t_0)$ $(\times 20)$ of the continuous tripole model with amplitude $\zeta_0 = 1$ and foci $f = 1/\sqrt{2}$, at $(a)$ the initial time $t_0 = 0$, and $(b)$ at $t_0 = 4240$. Contour intervals are $\Delta_\zeta = 0.2$ $(\zeta < 0)$ and $\Delta_\zeta = 1$ $(\zeta > 0)$. The black thick solid contour is the zero-vorticity isoline.

radius. However, the amplitude of these lateral vortices is small, and these embedded tripoles may be otherwise regarded as single stable elliptical vortices. Nevertheless, the presence of the lateral vortices is important to preserve the vortex ellipticity against vortex axis-symmetrization.

It is straightforward to extend the two-dipole tripole model to the superposition of $n \geqslant 3$ dipoles ($n$ equidistant lateral vortices with an azimuthal phase difference $\Delta\theta = 2\pi/n$). However, numerical experiments showed that these embedded $n$-dipoles were unstable and evolved into stable circular vortices.

These results may be relevant also to plasma physics, where tripolar vortices have been observed (Okamoto *et al.* 2003), as well as to baroclinic three-dimensional flows in the ocean (Pingree & Le Cann 1992). In fact, a three-dimensional quasi-geostrophic two-dipole tripole model is possible using exact quasi-geostrophic dipole solutions. Investigation along this line of research is left for future work.

## Acknowledgements

I thank three anonymous referees for their very helpful comments. Partial support for this study was obtained through project CTM2014-56987-P (Spanish Ministry of Science and Innovation).

## Supplementary movies

Supplementary movies are available at https://doi.org/10.1017/jfm.2019.730.

## Appendix A. Derivation of (3.10)

Expression (3.10) is the advection of the left (subscript $L$) vortex interior (subscript $i$) vorticity (including both modes 0 and 1) $\widetilde{\zeta}_{L0i} + \widetilde{\zeta}_{L1i}$, by the right (subscript $R$) vortex exterior (subscript $e$) velocity (including both modes 0 and 1) $\widetilde{\boldsymbol{u}}_{R0e} + \widetilde{\boldsymbol{u}}_{R1e}$, and is therefore equal to $(\widetilde{\boldsymbol{u}}_{R0e} + \widetilde{\boldsymbol{u}}_{R1e}) \cdot \boldsymbol{\nabla}(\widetilde{\zeta}_{L0i} + \widetilde{\zeta}_{L1i})$. The velocity and



https://doi.org/10.1017/jfm.2019.730 Published online by Cambridge University Press

vorticity gradient terms involved (which may be obtained from Viúdez 2019) are

$$\frac{\widetilde{\boldsymbol{u}}_{R0e}(x,y)}{\phi_0 \mathrm{J}_0(j_{1,1})} = \frac{1}{2}\left(\frac{j_{1,1}^2}{x_-^2+y^2} - 1\right)(-y\boldsymbol{e}_x + (x_-)\boldsymbol{e}_y), \tag{A 1}$$

$$\frac{\widetilde{\boldsymbol{u}}_{R1e}(x,y)}{\phi_1 \mathrm{J}_0(j_{1,1})} = j_{1,1}^2 \frac{yx_-}{(x_-^2+y^2)^2}\boldsymbol{e}_x - \frac{1}{2}\left(j_{1,1}^2 \frac{x_-^2-y^2}{(x_-^2+y^2)^2} + 1\right)\boldsymbol{e}_y, \tag{A 2}$$

$$\frac{\boldsymbol{\nabla}\widetilde{\zeta}_{L0i}(x,y)}{\phi_0} = \frac{\mathrm{J}_1(\sqrt{x_+^2+y^2})}{\sqrt{x_+^2+y^2}}((x_+)\boldsymbol{e}_x + y\boldsymbol{e}_y), \tag{A 3}$$

and

$$\frac{\boldsymbol{\nabla}\widetilde{\zeta}_{L1i}(x,y)}{\phi_1} = \left(x_+^2 \frac{\mathrm{J}_2(\sqrt{x_+^2+y^2})}{x_+^2+y^2} - \frac{\mathrm{J}_1(\sqrt{x_+^2+y^2})}{\sqrt{x_+^2+y^2}}\right)\boldsymbol{e}_x + y(x_+)\frac{\mathrm{J}_2(\sqrt{x_+^2+y^2})}{x_+^2+y^2}\boldsymbol{e}_y. \tag{A 4}$$

Performing the scalar product $(\widetilde{\boldsymbol{u}}_{R0e} + \widetilde{\boldsymbol{u}}_{R1e}) \cdot \boldsymbol{\nabla}(\widetilde{\zeta}_{L0i} + \widetilde{\zeta}_{L1i})$ and rearranging terms leads to (3.10).

## References


Abramowitz, M. & Stegun, I. 1964 *Handbook of Mathematical Functions*. Dover.

Carton, X. J., Flierl, G. R. & Polvani, L. M. 1989 The generation of tripoles from unstable axisymmetric isolated vortex structures. *Europ. Phys. Lett.* **9**, 339–344.

Chaplygin, S. A. 1903 One case of vortex motion in fluid. *Trans. Phys. Sect. Imperial Moscow Soc. Friends of Natural Sciences* **11** (N2), 11–14.

Dritschel, D. G. & Viúdez, A. 2003 A balanced approach to modelling rotating stably-stratified geophysical flows. *J. Fluid Mech.* **488**, 123–150.

Flierl, G. R., Stern, M. E. & Whitehead, J. A. 1983 The physical significance of modons: laboratory experiments and general integral constraints. *Dyn. Atmos. Oceans* **7**, 233–263.

Gutiérrez-Vega, J. C., Rodríguez-Dagnino, R. M., Meneses-Nava, M. A. & Chávez-Cerda, S. 2003 Mathieu functions, a visual approach. *Am. J. Phys.* **71**, 233–242.

van Heijst, G. J. F. & Kloosterziel, R. C. 1989 Tripolar vortices in a rotating fluid. *Nature* **338**, 569–571.

van Heijst, G. J. F., Kloosterziel, R. C. & Williams, C. W. M. 1991 Laboratory experiments on the tripolar vortex in a rotating fluid. *J. Fluid Mech.* **225**, 301–331.

Kizner, Z. & Khvoles, R. 2004 The tripole vortex: experimental evidence and explicit solutions. *Phys. Rev.* E **70**, 016307.

Lamb, H. 1895 *Hydrodynamics*, 2nd edn. Cambridge University Press.

McLachlan, N. W. 1951 *Theory and Application of Mathieu Functions*. Oxford Press.

Meleshko, V. V. & van Heijst, G. J. F. 1994 On Chaplygin's investigations of two-dimensional vortex structures in an inviscid fluid. *J. Fluid Mech.* **272**, 157–182.

Okamoto, A., Hara, K., Nagaoka, K., Yoshimura, S., Vranješ, J., Kono, M. & Tanaka, M. Y. 2003 Experimental observation of a tripolar vortex in a plasma. *Phys. Plasmas* **10** (6), 2211–2216.

Orlandi, P. & van Heijst, G. J. F. 1992 Numerical simulation of tripolar vortices in 2D flow. *Fluid Dyn. Res.* **9**, 179–206.

Pingree, R. D. & Le Cann, B. 1992 Three anticyclonic slope water oceanic eDDIES (SWODDIES) in the Southern Bay of Biscay in 1990. *Deep Sea Res.* **39**, 1147–1175.

Polvani, M. L. & Carton, X. J. 1990 The tripole: a new coherent vortex structure of incompressible two-dimensional flows. *Geophys. Astrophys. Fluid Dyn.* **51** (1–4), 87–102.

Viúdez, A. 2019 Azimuthal-mode solutions of two-dimensional Euler flows and the Chaplygin–Lamb dipole. *J. Fluid Mech.* **859**, R1.




https://doi.org/10.1017/jfm.2019.730 Published online by Cambridge University Press